3. M. T. Dillon, J. S. Good, K. J. Harrington, *Clin. Oncol.* **26**, 257–265 (2014).
4. A. Cieślar-Pobuda, Y. Saenko, J. Rzeszowska-Wolny, *Mutat. Res.* **732**, 9–15 (2012).
5. D. K. Klein *et al.*, *Nat. Commun.* **6**, 5800 (2015).
6. A. N. Kousholt *et al.*, *J. Cell Biol.* **197**, 869–876 (2012).
7. M. Enari *et al.*, *Nature* **391**, 43–50 (1998).
8. K. Samejima, W. C. Earnshaw, *Nat. Rev. Mol. Cell Biol.* **6**, 677–688 (2005).
9. R. A. V. Bell, L. A. Megeney, *Cell Death Differ.* **24**, 1359–1368 (2017).
10. B. D. Larsen, C. S. Sørensen, *FEBS J.* **284**, 1160–1170 (2017).
11. J. H. Song, K. Kandasamy, M. Zemskova, Y. W. Lin, A. S. Kraft, *Cancer Res.* **71**, 506–515 (2011).
12. J. D. Orth, A. Loewer, G. Lahav, T. J. Mitchison, *Mol. Biol. Cell* **23**, 567–576 (2012).
13. X. Liu *et al.*, *Cell Res.* **27**, 764–783 (2017).
14. G. Ichim *et al.*, *Mol. Cell* **57**, 860–872 (2015).
15. B. D. Larsen *et al.*, *Proc. Natl. Acad. Sci. U.S.A.* **107**, 4230–4235 (2010).
16. J. S. Brown, B. O'Carrigan, S. P. Jackson, T. A. Yap, *Cancer Discov.* **7**, 20–37 (2017).
17. J. Murai *et al.*, *Cancer Res.* **72**, 5588–5599 (2012).
18. X. Li *et al.*, *J. Biol. Chem.* **282**, 36177–36189 (2007).
19. M. H. Al-Khalaf *et al.*, *Cell Discov.* **2**, 15041 (2016).
20. V. Iglesias-Guimarais *et al.*, *J. Biol. Chem.* **288**, 9200–9215 (2013).
21. R. G. Syljuåsen *et al.*, *Cancer Res.* **64**, 9035–9040 (2004).
22. H. Sakahira, Y. Takemura, S. Nagata, *Arch. Biochem. Biophys.* **388**, 91–99 (2001).
23. S. M. Janicki *et al.*, *Cell* **116**, 683–698 (2004).
24. A. M. Sriramachandran *et al.*, *Mol. Cell* **78**, 975–985.e7 (2020).
25. C. Arnould, G. Legube, *J. Mol. Biol.* **432**, 724–736 (2020).
26. Y. Fu, M. Sinha, C. L. Peterson, Z. Weng, *PLOS Genet.* **4**, e1000138 (2008).
27. S. Walz *et al.*, *Nature* **511**, 483–487 (2014).
28. C. M. Torres *et al.*, *Science* **353**, aaf1644 (2016).
29. S. Matsuoka *et al.*, *Science* **316**, 1160–1166 (2007).
30. H. Jaiswal *et al.*, *EMBO J.* **36**, 2161–2176 (2017).
31. L. Galluzzi *et al.*, *Cell Death Differ.* **25**, 486–541 (2018).
32. A. Dréan, C. J. Lord, A. Ashworth, *Crit. Rev. Oncol. Hematol.* **108**, 73–85 (2016).
33. S. M. Harding *et al.*, *Nature* **548**, 466–470 (2017).
34. J. Chen *et al.*, *Cell Rep.* **32**, 108080 (2020).
35. A. R. Cortazar *et al.*, *Cancer Res.* **78**, 6320–6328 (2018).
36. M. Masutani, T. Nozaki, K. Wakabayashi, T. Sugimura, *Biochimie* **77**, 462–465 (1995).

ACKNOWLEDGMENTS

We thank the core facilities at BRIC for assistance; the CSS laboratory for insightful comments; A. H. Lund (Biotech Research and Innovation Centre, University of Copenhagen) for HCT116 p53 KO cells; D. Spector (Cold Spring Harbor Laboratory) for U2OS 263 cells; D. Durocher (Lunenfeld-Tanenbaum Research Institute) for mCherry-LacR expression plasmid; F. Zhang (McGovern Institute, Massachusetts Institute of Technology) for pSpCas9(BB)-2A-GFP and pSpCas9(BB)-2A-GFP plasmids; W. Earnshaw (Wellcome Centre for Cell Biology, University of Edinburgh) for murine CAD/ICAD coexpression plasmid (pRHS); and B. Singers Sørensen (University of Aarhus) for discussions and cell lines used during revision. **Funding:** Supported by Danish Cancer Society grants R90-A5949 (C.S.S.), R204-A12415 (J.Be.), and R204-A12617-B153 (J.Ba.); Danish Council for Independent Research grant 4004-00621 (C.S.S.); Novo Nordisk Foundation grants NNF16OC0022358 (C.S.S.) and NNF 0060590 (J.Ba.); Canadian Institute of Health Research grant 156120 (L.A.M.); a postdoctoral grant from Independent Research Fund Denmark (B.D.L.); Czech Science Foundation grant 19-07674S and Swiss National Science Foundation grant 310030_184716 (P.J.); Swedish Research council grant VR-MH 2014-46602-117891-30, Danish National Research Foundation (project CARD) grant DNRF 125, and Grant Agency of the Czech Ministry of Health grant NU21-03-00195 (J.Ba.); The European Union's Horizon 2020 program under the Marie Sklodowska-Curie grant (agreement 722729) (G.P.); and the Karolinska Institutet SFO for Molecular Biosciences, Vetenskapsrådet Junior Researcher grant 2015-04815, and H2020 ERC Starting Grant 715024 RAPID (S.J.E.). Bioinformatics analyses were performed on resources provided by the Swedish National Infrastructure for Computing (SNIC) at Uppmax server (projects SNIC 2020/15-9, SNIC 2020/6-3 to S.J.E.). **Author contributions:** Conceptualization: B.D.L., C.S.S. Methodology: B.D.L., J.Be., P.Y.K.Y., R.B., G.P., S.J.E., C.S.S. Experimental work: B.D.L., J.Be., P.Y.K.Y., R.B., G.P., V.U., J.K.A., T.T.K., S.E. Data documentation: B.D.L., J.Be., R.B., G.P., S.J.E., C.S.S. Data interpretation: B.D.L., J.Be., P.J., L.A.M., S.J.E., J.Ba., C.S.S. Funding acquisition: B.D.L., J.Be., P.J., L.A.M., S.J.E., J.Ba., C.S.S. Project administration: B.D.L., C.S.S. Supervision: B.D.L., P.J., L.A.M., S.J.E., J.Ba., C.S.S. Writing–original draft: B.D.L., J.Be., C.S.S. Writing–review and editing: B.D.L., J.Be., P.Y.K.Y., R.B., L.A.M., S.J.E., J.Ba., C.S.S. **Competing interests:** The authors declare that they have no competing interests. **Data and materials availability:** All materials are available upon request from C.S.S. All sequencing data and code are available at www.ncbi.nlm.nih.gov/geo/query/acc.cgi?acc=GSE171242 and https://doi.org/10.5281/zenodo.6386176.

SUPPLEMENTARY MATERIALS

science.org/doi/10.1126/science.abi6378
Materials and Methods
Figs. S1 to S13
Tables S1 and S2
Movies S1 and S2
References (*37*–*44*)
MDAR Reproducibility Checklist

30 March 2021; resubmitted 4 January 2022
Accepted 30 March 2022
10.1126/science.abi6378

NEUROSCIENCE

Molecular and neural basis of pleasant touch sensation

Benlong Liu[1]†, Lina Qiao[1]†‡, Kun Liu[1]†§, Juan Liu[1], Tyler J. Piccinni-Ash[1], Zhou-Feng Chen[1,2]*

Pleasant touch provides emotional and psychological support that helps mitigate social isolation and stress. However, the underlying mechanisms remain poorly understood. Using a pleasant touch–conditioned place preference (PT-CPP) test, we show that genetic ablation of spinal excitatory interneurons expressing prokineticin receptor 2 (PROKR2), or its ligand PROK2 in sensory neurons, abolishes PT-CPP without impairing pain and itch behaviors in mice. Mutant mice display profound impairments in stress response and prosocial behaviors. Moreover, PROKR2 neurons respond most vigorously to gentle stroking and encode reward value. Collectively, we identify PROK2 as a long-sought neuropeptide that encodes and transmits pleasant touch to spinal PROKR2 neurons. These findings may have important implications for elucidating mechanisms by which pleasant touch deprivation contributes to social avoidance behavior and mental disorders.

Our sense of touch is composed of discriminative and affective components. Discriminative touch detects physical properties of tactile stimuli (e.g., location, shape, texture, force, etc.), whereas affective touch conveys emotional value that is modulated by social context (*1*, *2*). Pleasant touch (e.g., cuddling, caressing, and hugging) encodes positive hedonic information that facilitates emotional development, affiliative behavior, and the well-being of social animals (*1*, *3*, *4*). Social touch is one of the most favored activities that might be evolutionarily conserved throughout the animal kingdom (*5*, *6*). In nonhuman primates, rodents, birds, and insects, allogrooming behavior (or allopreening for birds) is important for strengthening and maintaining social bonding, reciprocity, attachment, and hierarchy (*7*–*9*). Acute social isolation increases social cravings and reward-seeking behavior (*10*). Harlow's pioneering work demonstrated that infant rhesus monkeys separated from their mothers have an innate desire to cuddle soft cloth for contact comfort and emotional needs, and maternal touch is vital for the behavioral and psychological development of offspring (*11*). Likewise, long-term deprivation of maternal care and positive social touch has lasting negative consequences on the mental health of children (*12*, *13*). In fact, affective touch avoidance and deficiency are some of the hallmarks of several neuropsychiatric disorders, including autism spectrum disorders (ASDs) (*14*, *15*). Studies in humans have shown that C tactile (CT) fibers innervating hairy skin encode positive valence of social touch (*1*, *16*–*19*), whereas *MrgprB4*-expressing sensory neurons and *Gpr83*-expressing spinal projection neurons have been implicated in mice (*20*, *21*). Despite its profound importance, how pleasant touch information is encoded and transmitted from somatosensory neurons to the spinal cord remains unknown. Our understanding of the molecules and neural circuits of pleasant touch has been hampered by a paucity of suitable animal models and methodologies that permit accurate inference and assessment of the affective state of mice that experience pleasant touch. Unlike discriminative touch, affective touch mediated by unmyelinated C fibers is a slow process (*1*). We postulated that pleasant touch

[1]Center for the Study of Itch and Sensory Disorders and Department of Anesthesiology, Washington University School of Medicine, St. Louis, MO 63110, USA. [2]Departments of Medicine, Psychiatry, and Developmental Biology, Washington University School of Medicine, St. Louis, MO 63110, USA.
***Corresponding author. Email: chenz@wustl.edu**
†These authors contributed equally to this work.
‡Present address: Department of Biochemistry and Molecular Biology, Institute of Acupuncture and Moxibustion, China Academy of Chinese Medical Sciences, Beijing 100700, China.
§Present address: Department of Physiology, Institute of Acupuncture and Moxibustion, China Academy of Chinese Medical Sciences, Beijing 100700, China.

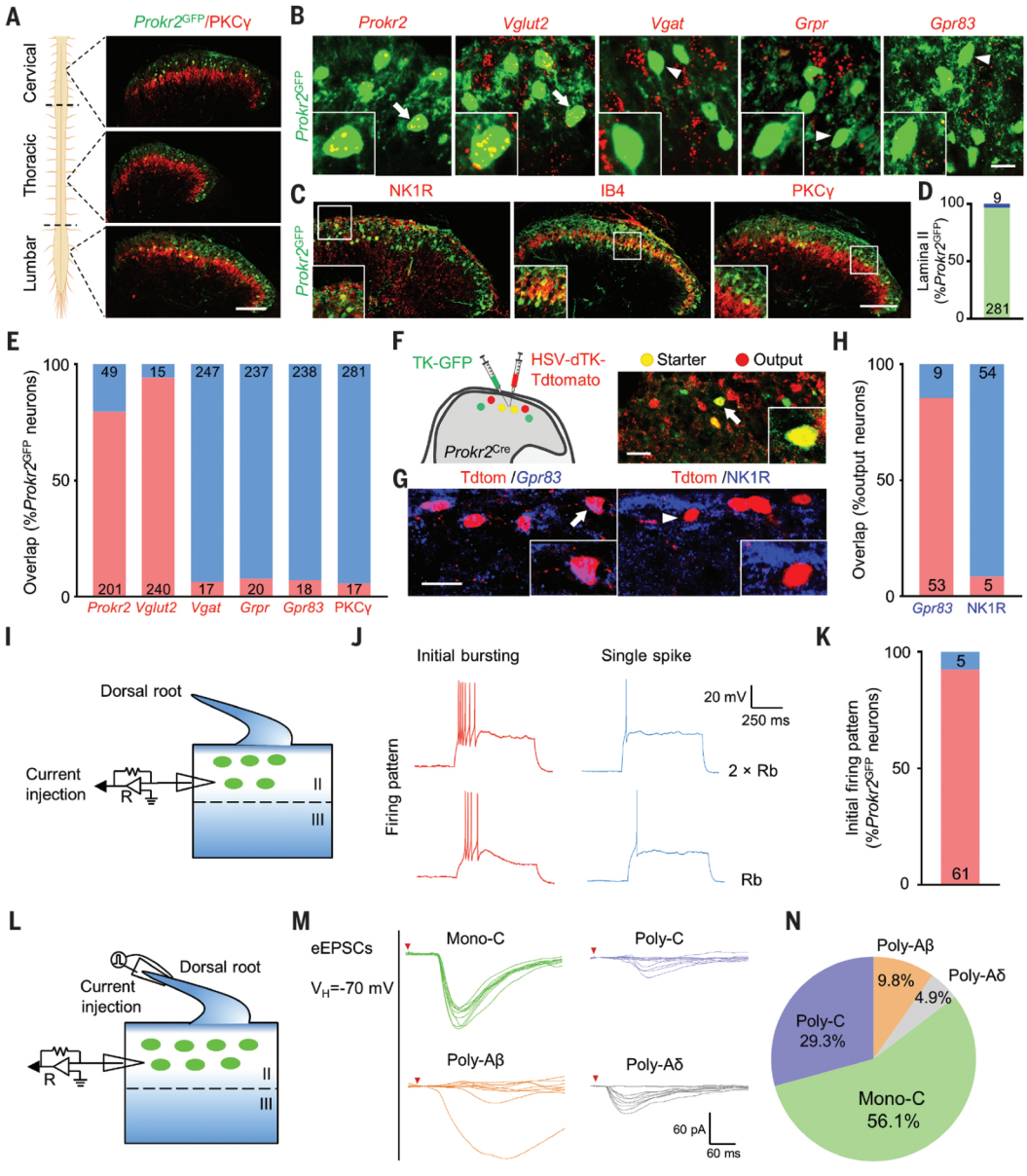

Fig. 1. PROKR2 neurons are a unique population of spinal excitatory interneurons. (**A** to **E**) Double staining of GFP with PKCγ at three levels of the spinal cord (A) and GFP with various markers in the lumbar cord [(B) and (C)]. Arrows indicate double-labeled cells, and arrowheads indicate GFP only. *n* = 3 mice. Scale bars, 100 μm [(A) and (C)] and 20 μm (B). (D) Quantification of (C), percentage of *Prokr2*^{GFP} cells in lamina II (green) and lamina I (blue). (E) Quantification of (B) and (C). Red in (E) indicates the percentage of double-labeled cells of *Prokr2*^{GFP} cells, and blue indicates GFP only. (**F**) Schematic of intraspinal injection of virus AAV5-Ef1a-DIO-EGFP-2a-TK-WPRE-pA (TK-GFP) and HSV-dTK-LSL-tdTomato (HSV-dTK-Tdtomato) in the dorsal horn of *Prokr2*^{Cre} mice at the lumbar level (left). (Right) Image showing virus expression in a starter neuron (yellow) expressing GFP and Tdtomato. Scale bar, 20 μm. (**G**) Double staining of *Gpr83* or NK1R anterogradely labeled with Tdtomato. Scale bar, 20 μm. (**H**) Quantification of (G). *n* = 3. (**I** to **K**) Schematic of the whole-cell patch-clamp recording of *Prokr2*^{GFP} neurons in the spinal cord slice preparations (I), a representative trace of the initial firing pattern (red) and single-spike firing pattern (blue) at 20 pA [rheobase (Rb)] and 40 pA [twofold rheobase (2 × Rb)] (J), and proportions of different types of firing pattern (K). *n* = 66 neurons. (**L** to **N**) Schematic of the recording of the type of inputs onto *Prokr2*^{GFP} neurons with dorsal root stimulation (L), representative traces of different types of inputs (M), and their proportions (N). eEPSCs, evoked excitatory postsynaptic currents. *n* = 41 neurons. All data are presented as means ± SEMs.

is encoded by slow-acting neuropeptides in C fibers and their cognate excitatory G protein–coupled receptors (GPCRs) in laminae II of the spinal cord that consist of microcircuits for relaying discrete sensory modalities from primary afferents to the brain (*22*). In a search for lamina- and modality-specific GPCRs, we found that prokineticin receptor 2 (PROKR2) is uniquely expressed in laminae II of the spinal cord, and PROKR2 neurons represent a previously unknown population of spinal excitatory interneurons. Using an unbiased behavioral paradigm in combination with physiological tests, extracellular recording, and genetic approaches, we sought to examine the role of the PROK2-PROKR2 signaling in pleasant touch.

Properties of spinal PROKR2-expressing lamina II excitatory interneurons

We used *Prokr2*^{GFP} transgenic mice as a surrogate to characterize PROKR2 expression in the spinal cord. RNAscope in situ hybridization (ISH) followed by immunohistochemical (IHC) studies indicated that green fluorescent protein (GFP) of *Prokr2*^{GFP} mice recapitulates a large part of *Prokr2* expression in laminae II (80.4%) of the spinal cord (Fig. 1, A to E). A significant fraction of GFP is distributed in the dorsal side of the lamina II inner (IIi) layer innervated by isolectin B4 (IB4)–binding non-peptidergic fibers (Fig. 1C). *Prokr2* is largely colocalized with the excitatory genes, like vesicular glutamate transporter 2 (*Vglut2*) (94.1%) and *Lmx1b* (96.8%), but rarely overlaps with the inhibitory neuronal markers, such as vesicular γ-aminobutyric acid (GABA) transporter (*Vgat*) (6.4%) or Pax2 (3.1%) (Fig. 1, B and E, and fig. S1, A and B). RNAscope ISH and IHC showed that *Prokr2* rarely overlaps with gastrin-releasing peptide receptor (*Grpr*) (7.8%), an itch-specific receptor expressed in laminae I and II interneurons (*23*, *24*), or protein kinase C γ (PKCγ) (5.7%), which labels the ventral side of the lamina IIi layer, with *Gpr83* (7.0%) or

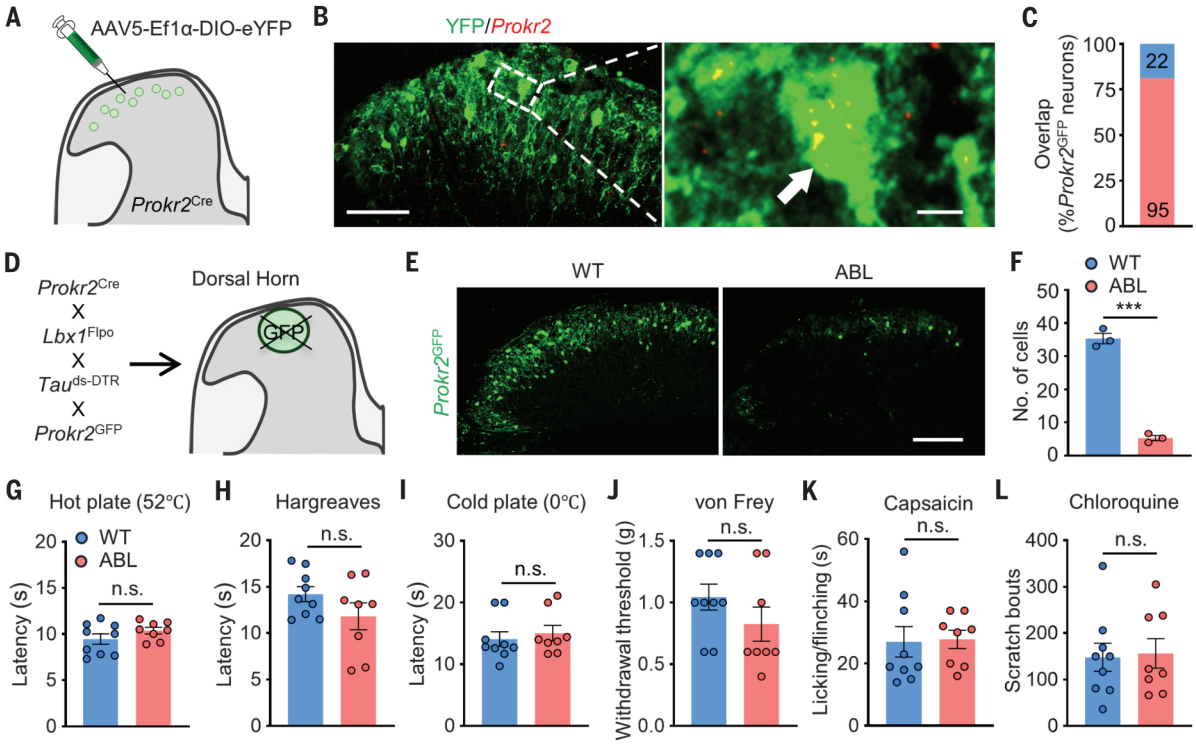

Fig. 2. PROKR2 neurons are dispensable for acute pain and itch behaviors. (**A**) Schematic of intraspinal injection of Cre-dependent adeno-associated virus (AAV) virus expressing YFP. (**B** and **C**) Double staining of YFP and *Prokr2* (arrow indicates a double-stained cell) in the lumbar cord (B) and percentage of overlapping cells (C). Scale bars, 50 μm (left) and 5 μm (right). (**D**) Strategy for intersectional genetic ablation of spinal *Prokr2*^{Cre} neurons. *Prokr2*^{Cre} mice were mated with *Lbx1*^{Flpo}, *Tau*$^{ds\text{-}DTR}$, and *Prokr2*^{GFP} lines to generate diphtheria toxin receptor (DTR)–expressing *Prokr2* neurons by injection of diphtheria toxin (50 μg/kg, i.p.). (**E** and **F**) Images of *Prokr2*^{GFP} neurons in WT and ABL mice (E) and quantification of *Prokr2*^{GFP} neurons (F). Scale bar, 150 μm. (**G** to **L**) Comparable latencies in hot plate (G), Hargreaves (H), and cold plate (I) tests; withdraw threshold in von Frey test (J); licking or flinching time induced by capsaicin (2 g, i.pl.) (K); and scratching numbers induced by chloroquine (200 μg, i.d.) (L) between WT and ABL mice. i.pl., intraplantar injection; i.p., intraperitoneal injection; i.d., intradermal injection. $n = 3$ (F); $n = 8$ to 9 [(G) to (L)]. Statistics by unpaired t test in (F) and (G) to (I). ***$P < 0.001$; n.s., not significant. Error bars indicate SEMs.

NK1R—two markers expressed in distinct subsets of projection neurons—implicated in affective touch and pain, respectively (*20*) (Fig. 1, B, C, and E). To identify the downstream target of PROKR2 neurons, we next performed Cre-dependent virus-mediated anterograde monosynaptic tracing in the spinal cord of *Prokr2*^{Cre} mice using HSV-dTK-LSL-tdTomato as the monosynaptic tracer to follow the output neurons (Fig. 1F). RNAscope ISH or IHC revealed that ~85.5% of the output neurons labeled by tdTomato express *Gpr83*, whereas only 8.5% express NK1R (Fig. 1, G and H).

We next examined whole-cell patch-clamp recordings of spinal cord slices obtained from *Prokr2*^{GFP} mice. The firing pattern of most *Prokr2*^{GFP} neurons was very homogeneous: ~92.4% displayed initial bursting firing, with a few neurons showing single-spike firing (Fig. 1, I to K). To identify the type of peripheral sensory inputs, we recorded the response of *Prokr2*^{GFP} neurons in the parasagittal section of spinal slices obtained from *Prokr2*^{GFP} mice with the dorsal root (L4 to L5) attached, using the dorsal root stimulation method as described previously (Fig. 1L) (*25*). *Prokr2*^{GFP} neurons predominantly receive monosynaptic and polysynaptic C fiber inputs (a combined 85.4%) with a small fraction of polysynaptic Aδ (4.9%) or Aβ inputs (9.8%) (Fig. 1, M and N). Furthermore, PROK2 application evoked subthreshold depolarizations in most *Prokr2*^{GFP} neurons, which were blocked by PKRA7, a PROKR2 antagonist (fig. S1, C and D).

PROKR2 neurons are dispensable for pain and itch transmission

To assess the function of spinal PROKR2 neurons, we first validated *Prokr2*^{Cre} mice by intraspinal injection of Cre-dependent yellow fluorescent protein (YFP) virus. Most *Prokr2*$^{Cre\text{-}GFP}$ neurons expressed *Prokr2* (81.2%) (Fig. 2, A to C). We then used an intersectional genetic strategy to ablate spinal PROKR2 neurons in *Prokr2*^{Cre} mice, hereafter referred to as ABL mice, as previously described (*25*) (Fig. 2, D to F, and fig. S2, A and B). The specificity of ablation was demonstrated by the loss of most *Prokr2*^{Cre} neurons (84.9%) and *Prokr2* (81.3%) without affecting PKCγ, neurokinin B (NKB), and *Grpr* in the spinal cord or *Prokr2*^{GFP} in discrete brain regions (Fig. 2, D to F; fig. S2, C and D; and fig. S3). A battery of pain and itch tests was conducted to assess the role of *Prokr2*^{Cre} neurons in somatosensory transmission. We did not observe a statistically significant difference in thermal pain, cold pain, mechanical thresholds, or inflammatory pain induced by capsaicin between ABL mice and their littermate control mice [referred to as wild-type (WT) mice; Fig. 2, G to K]. Chemical and mechanical itch as well as the hairy skin sensitivity to a sticky tape of ABL mice were comparable to those of WT mice (Fig. 2L and fig. S2, E and F).

PROKR2 neurons convey pleasant touch sensation

As a weak stimulus, gentle stroking with a soft brush on the hairy skin of mice does not elicit a robust motor response that can be used as a proxy to quantify pleasant touch sensation. Moreover, using a hand or soft brush to simulate pleasant touch in mice often causes avoidance behavior without habituation and conditioning. To circumvent these confounds, we developed a protocol that includes two procedural features to avoid the stress and

anxiety associated with handling. First, given that social isolation increases the urge for social touch and attachment (*26*), mice were single-housed for 1 week followed by week-long daily stroking sessions in the home cage. This procedure conditioned mice into a quiescent or inactive state upon gentle stroking, akin to pets being groomed (Fig. 3, A and B, and movies S1 to S3). Second, to increase the motivational drive to obtain rewards associated with pleasant touch (*27*), we performed eight conditioning sessions (one session per

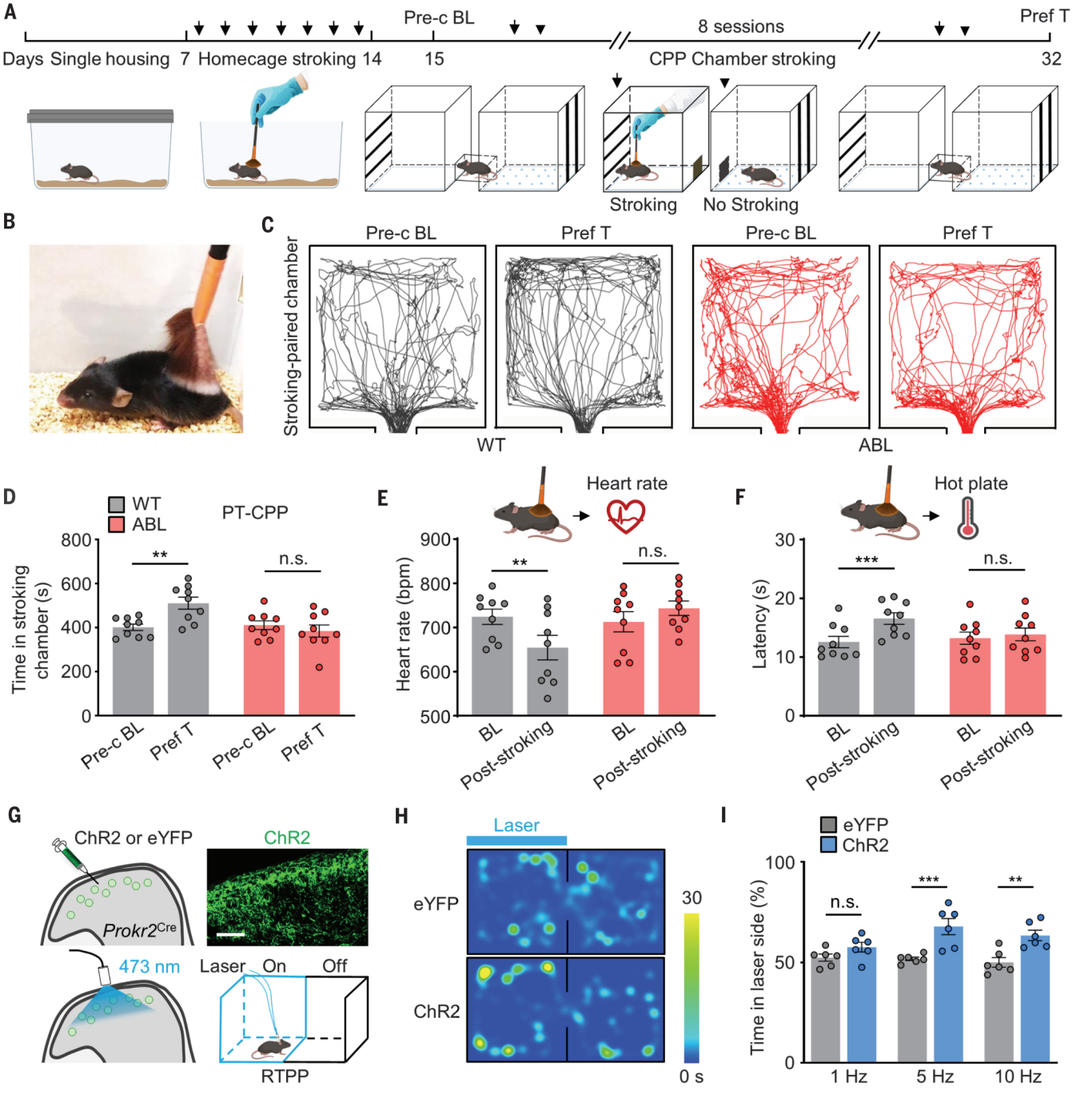

Fig. 3. PROKR2 neurons transmit pleasant touch sensation. (**A**) A schematic diagram of the experimental procedure for PT-CPP. (**B**) Photo of a mouse being stroked with a soft brush. (**C** and **D**) Representative trajectory plots (C) and time spent (D) in stroking-paired chamber for WT and ABL mice in the preconditioning baseline (Pre-c BL) and preference test (Pref T). Pre-c BL versus Pref T: $P < 0.01$ for WT and $P = 0.6822$ for ABL mice. (**E** and **F**) Heart rate (E) and thermal pain threshold (F) in the baseline and poststroking test. Heart rate, BL versus poststroking: $P < 0.01$ for WT and $P = 0.1563$ for ABL mice; hot plate, BL versus poststroking: $P < 0.001$ for WT and $P = 0.5206$ for ABL mice. bpm, beats per minute. (**G**) Schematic of intraspinal injection of Cre-dependent AAV virus expressing ChR2-eYFP or eYFP (top left) and image showing ChR2-eYFP in the cervical cord (top right). Schematic of real-time place preference test (RTPP) (bottom). Scale bar, 50 μm. (**H** and **I**) Representative heatmap (5 Hz) (H) and the percentage of time spent (I) in the chamber paired with the laser in the RTPP test. $n = 9$ [(D) to (F)]; $n = 6$ (I). Statistics by two-way repeated measures analysis of variance (ANOVA) followed by Bonferroni's multiple comparisons test [(D), (E), and (F)] or by two-way ANOVA followed by Bonferroni's multiple comparisons test (I). $^{**}P < 0.01$; $^{***}P < 0.001$; n.s., not significant. Error bars indicate SEMs.

2 days) using an unbiased two-chamber pleasant touch–conditioned place preference (PT-CPP) apparatus in which WT mice displayed no preference for either chamber (Fig. 3A, fig. S4B, and movie S4). On the test day, we performed a PT-CPP test to evaluate whether mice would spend more time in the chamber paired with gentle stroking than without. Both male and female mice developed PT-CPP as they spent significantly more time in the chamber paired with a soft brush (fig. S4, A, C, and D). These results demonstrate that gentle stroking in mice encodes the positive valence or hedonic value. In marked contrast to WT mice, ABL mice completely failed to show PT-CPP (Fig. 3, C and D), which indicates a profound loss of pleasant touch sensation. If PROKR2 neurons convey pleasant touch, their direct activation—in the absence of either primary afferent input or behavioral conditioning or context—should be positively reinforcing. We injected Cre-dependent channelrhodopsin-2 (ChR2) or enhanced YFP (eYFP) virus intraspinally into *Prokr2*^{Cre} mice followed by the real-time place preference test (RTPP) using optogenetics (Fig. 3G). Consistently, *Prokr2*$^{Cre\text{-}ChR2}$ mice preferred the chamber paired with photostimulation of PROKR2 neurons (5 and 10 Hz), whereas *Prokr2*$^{Cre\text{-}eYFP}$ mice showed no preference (Fig. 3, H and I). Together, these results demonstrate that PROKR2 neurons encode positive valence and rewarding value.

Apart from pleasant sensation (*1*), gentle stroking on the hairy skin of humans decreases heart rate (*28*) and pain sensation (*29*), reflecting a soothing state with a reduced level of stress (e.g., increasing the threshold for thermal pain). To ascertain whether mice might develop similar physiological changes, we measured the heart rate, thermal pain, and stress hormones after gentle stroking. Mice showed significantly reduced heart rates, increased thermal pain thresholds, and reduced plasma corticosterone levels (fig. S4, E to G). Consistent with behavioral studies, ABL mice displayed no significant reduction of the heart rate or analgesic effect in response to gentle stroking (Fig. 3, E and F). The lack of behavioral and physiological changes in ABL mice further demonstrates the crucial role of PROKR2 neurons in conveying pleasant touch.

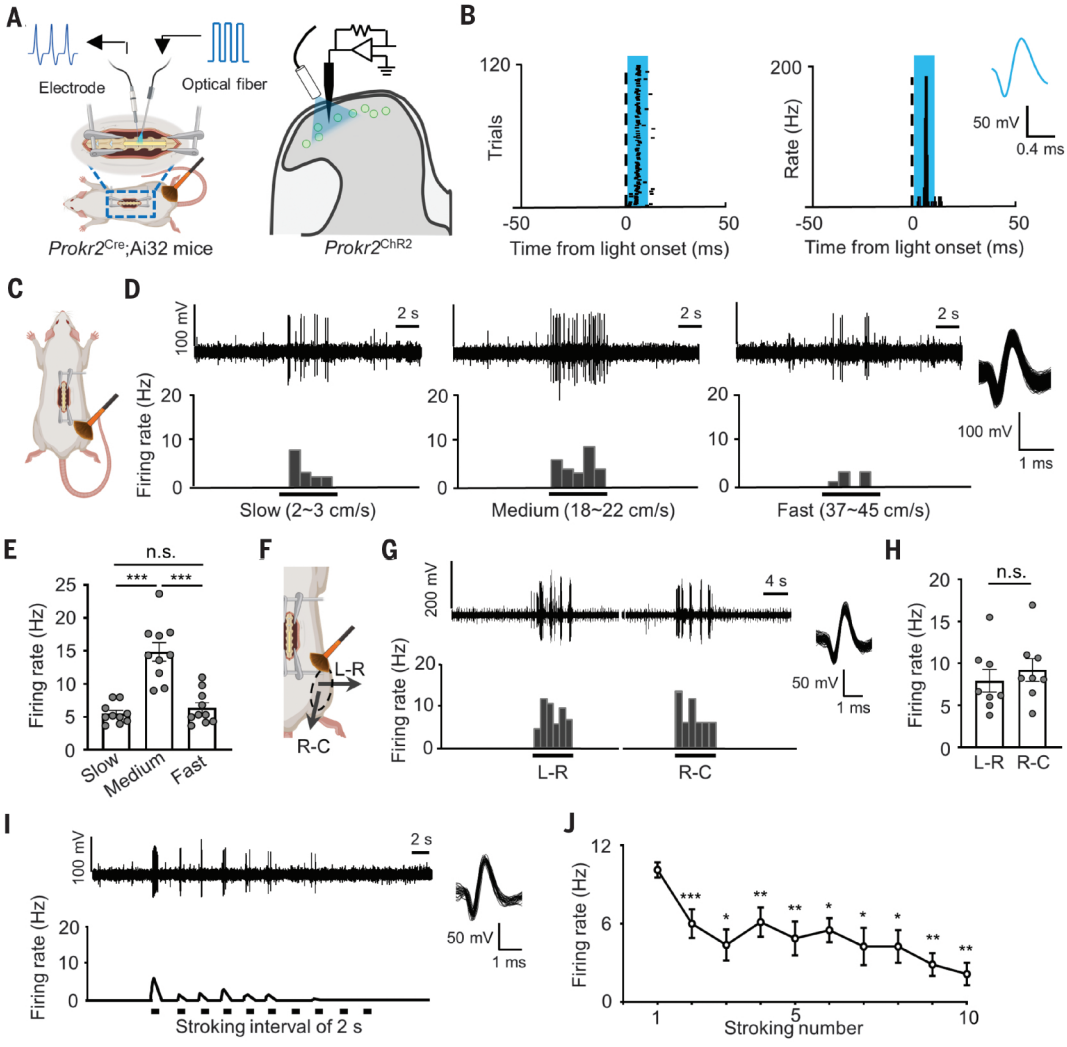

Fig. 4. PROKR2 neurons display characteristic features in response to gentle stroking. (**A**) (Left) Dorsal view of an anesthetized *Prokr2*^{Cre};Ai32 mouse showing the position of optical fiber and electrode implanted in the lumbar spinal cord. (Right) Cross-sectional view of the lumbar spinal cord showing optogenetic tagging of *Prokr2*^{ChR2} neurons in lamina II with blue lights on. (**B**) Example response of a PROKR2-expressing neuron to blue light activation. (Left) Spike raster showing multiple trials of laser stimulation at 1 Hz. (Right) The firing rate of one opto-tagged neuron within 10-ms light pulses. (Inset) Waveform on expanded time scale. Blue bar indicates a light pulse. (**C** to **E**) Schematic of brush stroking across the receptive field (C), representative traces (top) and corresponding peristimulus time histograms (PSTHs) (1-s bin) (bottom) (D), and firing rate (E) of *Prokr2*^{ChR2} neurons in response to a soft brush stroking moving at different speeds (slow, 2 to 3 cm/s; medium, 18 to 22 cm/s; fast, 37 to 45 cm/s) across the receptive field of hindlimb hairy skin. Dots represent spike rate of a single trial from individual neurons (E). (**F** to **H**) Schematic of brush stroking in different directions (F) (L-R: from left to right; R-C: from rostral to caudal), representative traces (top) and corresponding PSTHs (1-s bin) (bottom) (G), and firing rate (H) of spinal *Prokr2*^{ChR2} neurons in response to stroking in different directions. Brush stroking was applied across the receptive field of the hindlimb in different directions at a speed of 18 to 22 cm/s. (**I** and **J**) Representative trace (top) and corresponding PSTH (1-s bin) (bottom) (I) and firing rate (J) of spinal *Prokr2*^{ChR2} neurons in response to 10 repeated brush stroking stimuli with intervals of 2 s. (Inset) Superimposed waveforms on expanded time scale representing spikes of *Prokr2*^{ChR2} neurons evoked by stroking in (D), (G), and (I). n = 8 to 10 neurons from three to four mice. Statistics by one-way repeated measures ANOVA followed by Bonferroni post hoc [(E) and (J)] or by paired t test (H). *P < 0.05; **P < 0.01; ***P < 0.001; n.s., not significant. Error bars indicate SEMs.

Neurophysiological features of PROKR2 neurons in response to varying stimuli

To interrogate neural correlates of pleasant touch, we performed in vivo extracellular recording of the response of spinal PROKR2 neurons to gentle stroking using a soft brush moving across the receptive field in the hairy skin of the hindlimb of *Prokr2*^{Cre};Ai32 mice expressing ChR2-eYFP (Fig. 4A). Opto-tagged spinal neurons were classified as spinal *Prokr2*^{ChR2} neurons if they displayed reliable action potentials with a short response latency (10 ms) upon the delivery of a brief pulse of blue light (Fig. 4B) (*30*). Notably, the response of *Prokr2*^{ChR2} neurons was most vigorous when the hairy

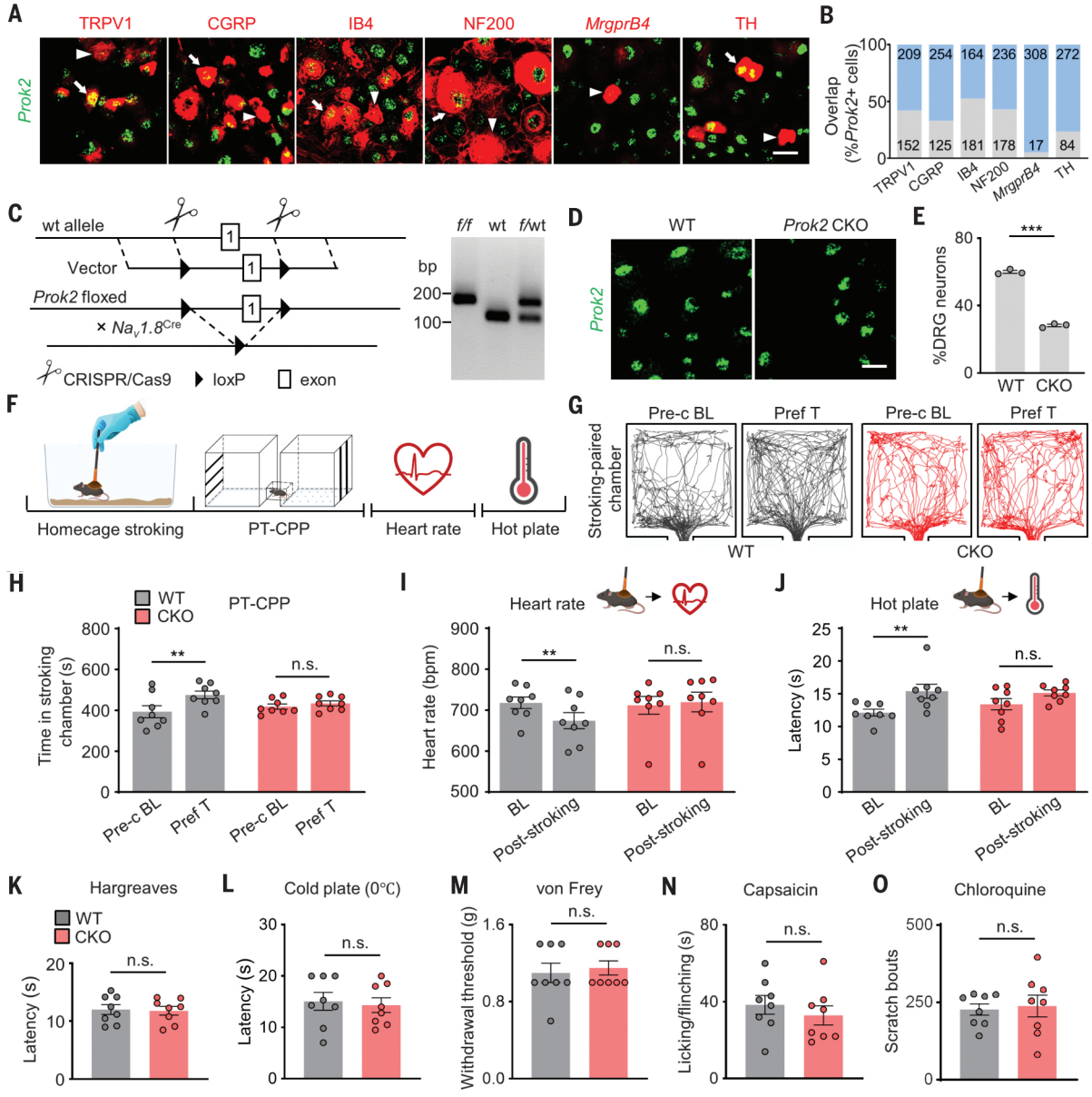

Fig. 5. Conditional deletion of *Prok2* in sensory neurons abolishes pleasant touch sensation. (**A**) Double staining of *Prok2* with various markers in DRG neurons. Arrows indicate double-stained cells, and arrowheads indicate *Prok2* only. Scale bar, 20 μm. (**B**) Overlapping percentages of (A). Gray indicates double-stained ratio, and blue indicates *Prok2* only. (**C**) (Left) Schematic of targeting strategy for generating *Prok2* floxed (*Prok2*$^{f/f}$) mice, which were mated with *Na*$_v$*1.8*^{Cre} mice to generate *Prok2*$^{f/f}$;*Na*$_v$*1.8*^{Cre} mice or *Prok2* CKO mice. (Right) Gel electrophoresis of genotyping polymerase chain reaction (PCR) from *Prok2*$^{f/f}$, wt/wt, and *Prok2*$^{f/wt}$ samples. (**D**) Expression of *Prok2* in DRGs of the control (*Prok2*$^{f/f}$, WT) and *Prok2* CKO mice (*Prok2*$^{f/f}$;*Na*$_v$*1.8*^{Cre}, CKO). Scale bar, 20 μm. (**E**) Quantification of (D). (**F**) A schematic of the experimental procedure. Parallel symbols indicate that PT-CPP, heart rate, and hot plate tests were performed independently after single-housing and home-cage stroking. (**G** and **H**) Representative trajectory plots (G) and time spent (H) in stroking-paired chamber for WT and CKO mice in the preconditioning baseline (Pre-c BL) and preference test (Pref T). Pre-c BL versus Pref T: $P < 0.01$ for WT and $P = 0.9552$ for CKO mice. (**I** and **J**) Heart rate test (I) and hot plate test (J) in WT and CKO mice. Heart rate, BL versus poststroking: $P < 0.01$ for WT and $P = 0.8737$ for CKO mice; hot plate, BL versus poststroking: $P < 0.01$ for WT and $P = 0.1531$ for CKO mice. (**K** to **O**) Comparable latencies in Hargreaves test (K) and cold plate test (L), withdraw threshold in von Frey test (M), licking or flinching time induced by capsaicin (2 g, i.pl.) (N), and scratching numbers induced by chloroquine injection (200 μg, i.d.) (O) between WT and CKO mice. $n = 3$ (E); $n = 8$ [(H) to (O)]. Statistics by unpaired t test [(E) and (K) to (O)] or by two-way repeated measures ANOVA followed by Bonferroni's multiple comparisons test [(H), (I), and (J)]. $^{**}P < 0.01$; $^{***}P < 0.001$; n.s., not significant. Error bars indicate SEMs.

skin of mice was brushed at a slowly moving speed (18 to 22 cm/s); however, their firing became sluggish if the stroking speed was slower (2 to 3 cm/s) or faster (37 to 45 cm/s) (Fig. 4, C and D). The mean firing rates at three brushing speeds exhibited an inverted U shape (Fig. 4E), reminiscent of that of human CT fibers (*17*, *18*). This prompted us to examine whether other features of *Prokr2*^{ChR2} neurons may resemble the hallmarks of human CT fibers (*1*, *16*, *17*, *19*). One signature of CT fibers is that they show no preference for orientation in the receptive field (*19*). *Prokr2*^{ChR2} neurons displayed comparable firing rates, irrespective of stroking directions (e.g., from rostral to caudal or from left to right; Fig. 4, F to H). Another distinctive feature is fatigue to the repetition of brush stroking, referring to gradually attenuated responses to repeated stroking stimuli within seconds (*1*, *16*, *17*, *19*). This feature distinguishes unmyelinated CT fibers from myelinated low-threshold mechanoreceptors (*18*) and has also been observed in cutaneous C mechanoreceptor afferents in rats (*31*) and cats (*32*). The firing rate of *Prokr2*^{ChR2} neurons also exhibited fatigue to repeated brush stroking and was reduced by 40.7 to 78.8% within 10 series of successive brush stroking (2-s interval) (Fig. 4, I and J). Consistent with a recent study showing the presence of CT afferents in human glabrous skin (*33*), PROKR2 neurons also responded to gentle stroking applied to the glabrous skin (fig. S5A), indicating the presence of PROK2 fibers in the glabrous skin.

At last, we examined several nongentle stroking–related stimuli that could elicit the response of CT fibers (*16*, *34*). Consistently, *Prokr2*^{ChR2} neurons responded to punctate stimulation (von Frey filament at 0.07 g or 0.7 mN), pinprick stimulation, and cooling temperature (30° to 15°C) (fig. S5, B to D).

Coding of pleasant touch by PROK2 in sensory neurons

We next examined *Prok2* expression in several types of dorsal root ganglion (DRG) neurons using RNAscope combined with IHC. *Prok2* partially overlaps to varying degrees with TRPV1 and calcitonin gene–related peptide (CGRP), which are expressed in nociceptive neurons; IB4; NF200, a neurofilament expressed predominantly in large-diameter neurons; *MrgprB4*; and tyrosine hydroxylase (TH) expressed in some C–low-threshold mechanoreceptors (C-LTMRs) (*35*) (Fig. 5, A and B, and fig. S6F). Overall, ~59.6% of DRG neurons express *Prok2*. To ascertain whether *Prok2*-expressing primary afferents form monosynaptic contacts with PROKR2 neurons, we performed rabies virus–mediated retrograde tracing in the spinal cord of *Prokr2*^{Cre} mice (*25*) (fig. S6, A and B). Examination of *Prok2* expression with retrograde transported glycoprotein (G)–deleted rabies virus (RVdG) that labels the input neurons with dsRed in DRGs revealed that ~70% of the input neurons were colabeled with *Prok2* (fig. S6, C to E). Only a small portion of CGRP fibers and minimal TRPV1 or TH fibers formed direct contacts with PROKR2 neurons, whereas no *MrgprB4* and IB4 afferents were found to form monosynaptic contacts with PROKR2 neurons (fig. S6, C and D). However, it should be noted that a lack of inputs from TH or IB4 afferents could be because of their resistance to rabies virus infection (*36*). Further, we show that the sizes of *Prok2* input neurons normally are in the 200-to-400-μm^2 range, which indicates that they are small DRG neurons (fig. S6E).

To determine the role of PROK2 in pleasant touch, we generated mice harboring a floxed allele of *Prok2* using the gene targeting strategy (Fig. 5C). Floxed *Prok2* mice were bred with *Na$_v$1.8*^{Cre} mice, which express the Cre recombinase in small nociceptive sensory neurons, to delete *Prok2* in *Na$_v$1.8*^{Cre} neurons of DRGs (Fig. 5C). The expression of *Prok2* was reduced by 52.8% without affecting IB4, CGRP, or *MrgprB4* in DRGs and IB4 or CGRP central fibers in the lumbar cord (Fig. 5, C to E, and fig. S7, A to D). Mice with conditional knockout of *Prok2* in DRGs, referred to as *Prok2* CKO mice, failed to show PT-CPP (Fig. 5, F to H). By contrast, they showed normal pain and itch behaviors (Fig. 5, K to O). Furthermore, *Prok2* CKO mice did not show significant changes in the heart rate and thermal pain thresholds after gentle stroking (Fig. 5, I and J). CT and C-LTMRs are insensitive to capsaicin, which activates TRPV1 fibers (*37*, *38*). This prompted us to explore the role of TRPV1 fibers in pleasant touch. Ablation of the central terminals of TRPV1 fibers with intrathecal resiniferatoxin (RTX), a potent TRPV1 agonist, abolished neurogenic pain elicited by capsaicin and markedly attenuated mechanical itch that is dependent on Aβ-LTMR and

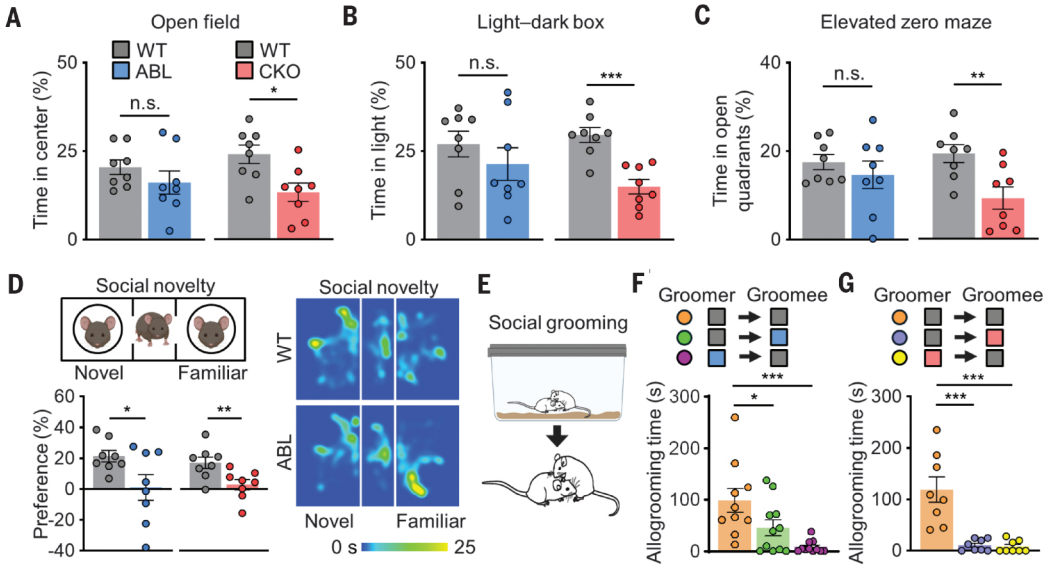

Fig. 6. Profound impairments of PROR2-PROKR2 mutant mice in stress response and prosocial behaviors. (**A** to **C**) Stress and anxiety-like behavioral tests. Shown are the percentages of time spent in the center zone of the open field apparatus (A), time spent in the light-illuminated chamber of the light-dark box (B), and time spent in the open quadrants of the elevated zero maze (C). WT versus ABL: $P = 0.2795$ (A), $P = 0.3514$ (B), and $P = 0.4312$ (C); WT versus CKO: $P < 0.05$ (A), $P < 0.001$ (B), and $P < 0.01$ (C). (**D**) The three-chamber social novelty test. The preference index for the percentage of time spent exploring the chamber with an unfamiliar mouse versus a familiar mouse (left). (Right) Representative heatmaps of locomotor activity in the chambers. WT versus ABL: $P < 0.05$; WT versus CKO: $P < 0.01$. (**E** to **G**) The home-cage social grooming test. Cartoons show mouse allogrooming in the home cage (E). (F and G) Allogrooming time for each pair. Groomer-groomee (F), WT-WT pair versus WT-ABL pair: $^*P < 0.05$; WT-WT pair versus ABL-WT pair: $^{***}P < 0.001$. Groomer-groomee (G), WT-WT pair versus WT-CKO pair: $^{***}P < 0.001$; WT-WT pair versus CKO-WT pair: $^{***}P < 0.001$. $n = 8$ [(A) to (D) and (G)]; $n = 10$ to 11 (F). Statistics by unpaired t test [(A) to (D)] or one-way ANOVA followed by Bonferroni post hoc [(F) and (G)]. $^*P < 0.05$; $^{**}P < 0.01$; $^{***}P < 0.001$; n.s., not significant. Error bars indicate SEMs.

C fiber inputs and GRP and GRPR neurons (*22*, *25*) (fig. S8, A to D). Notably, RTX treatment had no effect on PT-CPP (fig. S8, E to G).

Profound deficits in stress response and prosocial behaviors of PROK2 mutant mice

Pleasant social touch affords tremendous emotional and psychological benefits by indirectly activating the endogenous reward-pleasure circuits to release a plethora of neuropeptides and neurotransmitters that encode antistress, positive hedonic, and prosocial value (*1*, *7*, *39*–*42*). We sought to examine whether a loss of pleasant touch developmentally or in adult mice may result in abnormal stress responses. *Prok2* CKO mice spent significantly less time than their WT littermates in the center zone of the open-field apparatus, in the light-illuminated chamber of the light-dark box, and in the open quadrants of the elevated zero maze apparatus (Fig. 6, A to C). By contrast, the time that ABL mice spent in these areas did not differ from that of their WT littermates (Fig. 6, A to C). We further assessed social novelty recognition of mutant mice using the three-chamber social interaction test. Unlike WT mice, neither *Prok2* CKO nor ABL mice displayed a preference for a newly introduced mouse, demonstrating severe deficits in social novelty recognition (Fig. 6D and fig. S9).

Finally, we evaluated whether *Prok2* CKO or ABL mice might have deficits in social touch behavior. To examine this, we first monitored spontaneous social interactions between C57BL-6J paired adult mice in the home cage, which subserves a more naturalistic environment, and observed frequent social or allogrooming behaviors unrelated to sexual or aggressive and/or conflict activity (Fig. 6E and movie S5). In sharp contrast to the paired WT-WT conspecifics, social grooming of WT mice toward ABL mice was significantly diminished (Fig. 6F). Unexpectedly, ABL mice rarely groomed WT conspecifics capable of sensing pleasant touch (Fig. 6F). These deficits were even more pronounced in the WT–*Prok2* CKO pairs (Fig. 6G).

Discussion

Using an interdisciplinary approach coupled with autonomic, neuroendocrine, electrophysiological, and behavioral criteria, our study demonstrates the crucial function of the PROK2-PROKR2 signaling pathway in pleasant touch. The profound loss of pleasant touch sensation in *Prok2* CKO mice underscores the pivotal role of PROK2 in the coding and transmitting of pleasant touch information. Our work reveals two parallel peptidergic pathways, distinguished by their capsaicin sensitivity, from the skin to the spinal cord: One conveys positive valence to PROKR2 interneurons, which constitutes an obligate circuit for sending pleasant touch to the brain via *Gpr83* neurons, and the other conveys negative valence to the brain through spinal pain- and itch-specific local microcircuits and NK1R projection neurons (*20*, *24*, *43*). We argue that PROK2 in Aβ and Aδ fibers is unlikely to be involved in pleasant touch because PROKR2 neurons receive no direct inputs from these fibers. Moreover, unlike unmyelinated C fibers that encode the specificity of sensory modalities through slow-acting neuropeptides, myelinated Aβ and Aδ fibers typically use fast-acting glutamate as a neurotransmitter to relay information (*22*). We establish the function of PROK2 in encoding affective properties of gentle stroking; however, understanding how Aβ and Aδ LTMR fibers contribute to the transmission of discriminative properties of gentle touch and stroking will require further studies. Although PROK2 fibers that synapse with PROKR2 neurons could be the equivalent of human CT fibers, it is not feasible to examine their conduction velocities or cutaneous innervation patterns in isolation. Nonetheless, notable neurophysiological features shared by PROKR2 neurons and human CT fibers indicate that a subset of PROK2 fibers is equivalent to CT fibers. The response of PROKR2 neurons to cooling raises the possibility that PROKR2 neurons may be a convergent node for integrating different kinds of cutaneous information that encodes positive hedonic valence (e.g., pleasantness of cooling), akin to GRPR neurons subserving as a convergent node for mechanical and chemical itch (*25*). These data further support the neuropeptide code model that somatosensory modalities with slow response kinetics are encoded by neuropeptides in sensory neurons and conveyed by respective spinal microcircuits that can be defined and identifiable through specific GPCR expression (*22*). The development of the PT-CPP test that entails inference of pleasant touch in an unbiased manner overcomes a major obstacle in the interrogation of molecular underpinnings and neural circuits of pleasant touch. Together with the ethologically relevant seminaturalistic social grooming paradigm, we provide an avenue to unravel mechanisms by which the need for affective touch drives social attachment and affiliative behaviors.

This study has important clinical implications. The heightened stress and anxiety-like behaviors of *Prok2* CKO but not ABL mice are attributable to a lack of pleasant touch during a critical period in development, which supports prior studies showing that early tactile experience is more instrumental in shaping the resilience of offspring against stressful events (*44*, *45*). Accordingly, ABL mice are less vulnerable to stress. In light of the challenge in the study of the developmental role of pleasant touch because of the multisensory nature of parental care (*46*), *Prok2* CKO mice might serve as an invaluable animal model for assessment of the long-term effects of deprivation of maternal or caregiving nurturing touch on offsprings' development and health (*47*). A dearth of pleasant touch sensation could dysregulate prosocial neuropeptide expression in the brain and thereby impede social recognition and interactions. The failure of mutant mice to recognize unfamiliar conspecifics indicates a crucial role of pleasant touch in social recognition and social memory known to be important for social bonding (*48*). Additionally, the marked avoidance of the social touch phenotype is reminiscent of some early traits of ASD (*10*, *14*, *49*). Further analysis of prosocial behavioral impairment in *Prok2* CKO mice may offer additional insights into the etiology of certain neurodevelopmental and affective disorders that hinder social interactions and affiliative behaviors. The inability of mutant mice to groom WT conspecifics stresses the importance of PROK2 signaling in mediating synchronous and bidirectional communication of mutually beneficial social information through reciprocal tactile contacts (*6*). Finally, the observation that the firing features of PROKR2 neurons recapitulate the hallmarks of human CT fibers reinforces the notion that neural mechanisms of pleasant touch are conserved between humans and rodents. Conceivably, a deficiency of PROK2-PROKR2 signaling might result in social and emotional impairments that could lead to social isolation, anxiety, and mental disorders.

REFERENCES AND NOTES

1. F. McGlone, J. Wessberg, H. Olausson, *Neuron* **82**, 737–755 (2014).
2. V. E. Abraira, D. D. Ginty, *Neuron* **79**, 618–639 (2013).
3. I. Morrison, L. S. Löken, H. Olausson, *Exp. Brain Res.* **204**, 305–314 (2010).
4. A. Montagu, *Touching: The Human Significance of the Skin* (Harper Collins, ed. 3, 1986).
5. J. Panksepp, *Affective Neuroscience: The Foundations of Human and Animal Emotions* (Affective Science Series, Oxford Univ. Press, 1998).
6. M. J. Hertenstein, J. M. Verkamp, A. M. Kerestes, R. M. Holmes, *Genet. Soc. Gen. Psychol. Monogr.* **132**, 5–94 (2006).
7. R. I. M. Dunbar, *Neurosci. Biobehav. Rev.* **34**, 260–268 (2010).
8. F. B. M. de Waal, M. Suchak, *Phil. Trans. R. Soc. B* **365**, 2711–2722 (2010).
9. E. O. Wilson, *Sociobiology: The New Synthesis* (Harvard Univ. Press, 1975).
10. C. J. Cascio, D. Moore, F. McGlone, *Dev. Cogn. Neurosci.* **35**, 5–11 (2019).
11. H. F. Harlow, *Am. Psychol.* **13**, 673–685 (1958).
12. R. A. Spitz, *Psychoanal. Study Child* **1**, 53–74 (1945).
13. J. Bowlby, *Bull. World Health Organ.* **3**, 355–533 (1951).
14. A. C. Voos, K. A. Pelphrey, M. D. Kaiser, *Soc. Cogn. Affect. Neurosci.* **8**, 378–386 (2013).
15. M. D. Thye, H. M. Bednarz, A. J. Herringshaw, E. B. Sartin, R. K. Kana, *Dev. Cogn. Neurosci.* **29**, 151–167 (2018).
16. Å. Vallbo, L. Löken, J. Wessberg, in *Affective Touch and the Neurophysiology of CT Afferents*, H. Olausson, J. Wessberg, I. Morrison, F. McGlone, Eds. (Springer, 2016), pp. 1–30.
17. L. S. Löken, J. Wessberg, I. Morrison, F. McGlone, H. Olausson, *Nat. Neurosci.* **12**, 547–548 (2009).
18. A. B. Vallbo, H. Olausson, J. Wessberg, *J. Neurophysiol.* **81**, 2753–2763 (1999).
19. J. Wessberg, H. Olausson, K. W. Fernström, A. B. Vallbo, *J. Neurophysiol.* **89**, 1567–1575 (2003).
20. S. Choi *et al.*, *Nature* **587**, 258–263 (2020).
21. S. Vrontou, A. M. Wong, K. K. Rau, H. R. Koerber, D. J. Anderson, *Nature* **493**, 669–673 (2013).
22. Z. F. Chen, *Nat. Rev. Neurosci.* **22**, 758–776 (2021).
23. Y. G. Sun, Z. F. Chen, *Nature* **448**, 700–703 (2007).

24. Y. G. Sun *et al*., *Science* **325**, 1531–1534 (2009).
25. S. Chen *et al*., *Nat. Commun.* **11**, 5074 (2020).
26. E. B. Keverne, N. D. Martensz, B. Tuite, *Psychoneuroendocrinology* **14**, 155–161 (1989).
27. C. L. Cunningham, C. M. Gremel, P. A. Groblewski, *Nat. Protoc.* **1**, 1662–1670 (2006).
28. R. Pawling, P. R. Cannon, F. P. McGlone, S. C. Walker, *PLOS ONE* **12**, e0173457 (2017).
29. L. L. Meijer, C. Ruis, M. J. van der Smagt, E. J. A. Scherder, H. C. Dijkerman, *J. Neuropsychol.* **16**, 38–53 (2022).
30. J. P. Fadok *et al*., *Nature* **542**, 96–100 (2017).
31. J. W. Leem, W. D. Willis, J. M. Chung, *J. Neurophysiol.* **69**, 1684–1699 (1993).
32. A. Iggo, *J. Physiol.* **152**, 337–353 (1960).
33. R. H. Watkins *et al*., *J. Neurophysiol.* **125**, 232–237 (2021).
34. M. Nordin, *J. Physiol.* **426**, 229–240 (1990).
35. L. Li *et al*., *Cell* **147**, 1615–1627 (2011).
36. G. W. Albisetti *et al*., *J. Neurosci.* **37**, 10358–10371 (2017).
37. F. McGlone, S. Walker, R. Ackerley, in *Affective Touch and the Neurophysiology of CT Afferents*, H. Olausson, J. Wessberg, I. Morrison, F. McGlone, Eds. (Springer, 2016), pp. 265–282.
38. M. J. Caterina *et al*., *Nature* **389**, 816–824 (1997).
39. K. Uvnäs-Moberg, L. Handlin, M. Petersson, *Front. Psychol.* **5**, 1529 (2015).
40. J. Panksepp, B. H. Herman, T. Vilberg, P. Bishop, F. G. DeEskinazi, *Neurosci. Biobehav. Rev.* **4**, 473–487 (1980).
41. H. Yu *et al*., *Neuron* **110**, 1051–1067.e7 (2022).
42. Y. Tang *et al*., *Nat. Neurosci.* **23**, 1125–1137 (2020).
43. D. Mu *et al*., *Science* **357**, 695–699 (2017).
44. M. J. Meaney, *Annu. Rev. Neurosci.* **24**, 1161–1192 (2001).
45. A. Kaffman, M. J. Meaney, *J. Child Psychol. Psychiatry* **48**, 224–244 (2007).
46. C. Dulac, L. A. O'Connell, Z. Wu, *Science* **345**, 765–770 (2014).
47. F. S. Hall, *Crit. Rev. Neurobiol.* **12**, 129–162 (1998).
48. H. Walum, L. J. Young, *Nat. Rev. Neurosci.* **19**, 643–654 (2018).
49. K. L. Bales *et al*., *Neurosci. Biobehav. Rev.* **95**, 202–219 (2018).

ACKNOWLEDGMENTS

We thank X. Liu for technical help, Y. Zhang and F. Gao for help with viral tracing, Q. Ma and M. Goulding for providing *Lbx1*^{Flpo} and *Tau*$^{ds\text{-}DTR}$ lines, L. Setton and T. McGrath for help with the initial design of the stroking test, and R. Bardoni for discussion. **Funding:** The project has been supported by NIH grants 1R01AR056318-06 and R01NS094344 (to Z.-F.C.). **Author contributions:** B.L. performed immunostaining, genetic ablation, and electrophysiological studies. L.Q. and K.L. developed the PT-CPP test and performed in vivo extracellular recording. J.L. performed RNAscope and double staining. T.J.P.-A. participated in the behavioral tests. B.L., L.Q., and Z.-F.C. wrote the manuscript. Z.-F.C. conceived and supervised the project. **Competing interests:** The authors declare no competing interests. **Data and materials availability:** All data are available in the main text or the supplementary materials.

SUPPLEMENTARY MATERIALS

science.org/doi/10.1126/science.abn2479
Materials and Methods
Figs. S1 to S9
References (*50*–*69*)
MDAR Reproducibility Checklist
Movies S1 to S5

13 November 2021; accepted 24 March 2022
10.1126/science.abn2479

ZEOLITES

In situ imaging of the sorption-induced subcell topological flexibility of a rigid zeolite framework

Hao Xiong[1]†, Zhiqiang Liu[2]†, Xiao Chen[1]*, Huiqiu Wang[1], Weizhong Qian[1], Chenxi Zhang[1]*, Anmin Zheng[2], Fei Wei[1]*

The crystallographic pore sizes of zeolites are substantially smaller than those inferred from catalytic transformation and molecular sieving capabilities, which reflects flexible variation in zeolite opening pores. Using in situ electron microscopy, we imaged the straight channels of ZSM-5 zeolite with benzene as a probe molecule and observed subcell flexibility of the framework. The opening pores stretched along the longest direction of confined benzene molecules with a maximum aspect change of 15%, and the *Pnma* space group symmetry of the MFI framework caused adjacent channels to deform. This compensation maintained the stability and rigidity of the overall unit cell within 0.5% deformation. The subcell flexibility originates mainly from the topologically soft silicon-oxygen-silicon hinges between rigid tetrahedral SiO_4 units, with inner angles varying from 135° to 153°, as confirmed by ab initio molecular dynamics simulations.

Zeolite pores, which have diameters ranging from ~0.3 to ~1.3 nm, dictate their molecular sieving properties and control access to internal sites that are catalytically active or preferred for binding by sorbates (*1*–*4*). By adjusting the size and shape of pore openings, the size and shape of adsorbing molecules that fit inside the pores can be selected, thereby excluding larger molecules. This effect is exploited in selective chemical conversion (*4*–*9*). However, the effective pore sizes calculated from the crystallographic structures are substantially smaller than those inferred from catalytic transformation and molecular sieving capabilities (*8*–*10*). It has long been speculated that this discrepancy reflects in part a flexible deformation of zeolite pores.

Nonetheless, the flexible deformation of zeolite pores is rarely reported. Unlike flexible metal-organic frameworks (MOFs) with long and soft organic linkers (*11*–*13*), zeolite materials (with an elastic modulus in the range of 50 to 100 GPa) macroscopically behave as rigid and fragile materials in most applications (*14*–*16*). Findings related to zeolite flexibility have included minor variations in cell parameters (<10 pm) and a symmetry transformation from monoclinic to orthorhombic as a function of temperature and sorbates (*17*–*23*).

Direct measurement of pore sizes is, in principle, possible by diffraction, such as x-ray diffraction and electron diffraction. Nonetheless, the derived Debye-Waller factors for zeolites usually compensate for the complexity of zeolite crystal structures and various other model deficiencies, including inhomogeneity effects. Furthermore, averaged cell-scale results cannot indicate the local structure of deformed opening pores caused by successive twisted tetrahedrons. Crystal dynamics simulation techniques have been applied to trace the motion and vibration of specific atoms within zeolite frameworks, and some progress toward describing framework flexibility has been made, but supporting experimental evidence has been lacking (*2*, *9*, *24*–*26*). Thus, new experimental technology with ultrahigh spatial resolution is needed to reveal the subcell local structural evolution of the zeolite framework when guest molecules break through the pore size limit, especially in practical applications.

Integrated differential phase contrast scanning transmission electron microscopy (iDPC-STEM) can reveal the local structures of zeolites and image the confined molecules inside them in real space at an atomic scale (*27*–*30*) because of its excellent capability for imaging light and heavy elements together (*31*, *32*). Here, we combined iDPC-STEM imaging with an in situ atmosphere system to monitor the molecular phase transition and corresponding geometric variations of opening pores during the benzene adsorption-desorption process in real time. We studied the straight channel (5.3 Å × 5.6 Å) of ZSM-5 (MFI-type) zeolite as the imaging window and used benzene, which has a kinetic diameter of 5.85 Å, as a probe molecule. We observed the phase transition of confined benzene molecules and resolved the varying atomic structure of the MFI framework. Thus, we successfully observed the subcell flexibility of the zeolite framework, investigated the local deformation of zeolite channels, and monitored the dynamic evolution process when guest molecules enter or exit the zeolite framework. The results will enable us to better understand the topologically flexible structural characteristics of zeolites and the intrinsic mechanism of molecular diffusion in microporous materials.

[1]Beijing Key Laboratory of Green Chemical Reaction Engineering and Technology, Department of Chemical Engineering, Tsinghua University, Beijing 100084, China. [2]State Key Laboratory of Magnetic Resonance and Atomic and Molecular Physics, National Center for Magnetic Resonance in Wuhan, Innovation Academy for Precision Measurement Science and Technology, Chinese Academy of Sciences, Wuhan 430071, China.
***Corresponding author. Email: chenx123@mail.tsinghua.edu.cn (X.C.); cxzhang@mail.tsinghua.edu.cn (C.Z.); wf-dce@mail.tsinghua.edu.cn (F.W.)**
†These authors contributed equally to this work.